



Evolution over two decades of the tropical clouds in a subsidence area and their relation to large-scale environment

Marjolaine Chiriaco, Hélène Chepfer, Mathieu Reverdy, G. Cesana

► To cite this version:

Marjolaine Chiriaco, Hélène Chepfer, Mathieu Reverdy, G. Cesana. Evolution over two decades of the tropical clouds in a subsidence area and their relation to large-scale environment. 2012. hal-00856000

HAL Id: hal-00856000

<https://hal.science/hal-00856000>

Preprint submitted on 30 Aug 2013

HAL is a multi-disciplinary open access archive for the deposit and dissemination of scientific research documents, whether they are published or not. The documents may come from teaching and research institutions in France or abroad, or from public or private research centers.

L'archive ouverte pluridisciplinaire **HAL**, est destinée au dépôt et à la diffusion de documents scientifiques de niveau recherche, publiés ou non, émanant des établissements d'enseignement et de recherche français ou étrangers, des laboratoires publics ou privés.

1 **Evolution over two decades of the tropical clouds in a subsidence area and their**
2 **relations to large-scale environment**

3

4 M. Chiriaco⁽¹⁾, H. Chepfer⁽²⁾, M. Reverdy⁽³⁾, G. Cesana⁽²⁾

5 (1) : LATMOS/IPSL, Université de Versailles Saint Quentin, France

6 (2) : LMD/IPSL, Université Pierre et Marie Curie, France

7 (3) : LMD/IPSL, Ecole Polytechnique, France

8

9

10 Submitted to Journal of Geophysical Research

11 Contact: Marjolaine Chiriaco, marjolaine.chiriaco@latmos.ipsl.fr

12 LATMOS

13 11 Boulevard d'Alembert

14 78280 Guyancourt

15 France

16

17
18

Abstract

19 The interannual variability of cloud properties in a tropical subsidence area (South
20 Atlantic Ocean) is examined using 23 years of ISCCP cloud fractions and optical depths,
21 complemented with ISCCP/Meteosat visible reflectance and a four-years comparison with
22 CALIPSO-GOCCP products. The mean seasonal cloud properties are examined in the area, as
23 their interannual evolution. Circulation regimes (characterized with the SST and w_{500} from
24 NCEP and ERA-Interim) that dominate summer and winter are also examined, and
25 atmospheric situations are classified in five circulation regimes: ascending air masses, and
26 moderate or strong subsidence with warm or cold SSTs. We examine the mean cloud cover,
27 optical depth, and reflectance in each regime and their evolution in time over 23 years.
28 Observational results (mean values and interannual variability) are compared with simulations
29 from the IPSL and CNRM climate models (part of the CMIP5 experiment), using simulators
30 to ensure that differences can be attributed to model defects.

31 It results that regime occurrence strongly depends on the dataset (NCEP or ERA-
32 Interim), as do their evolution in time along 23 years. The observed cloud cover is stable in
33 time and weakly regime-dependent, whereas the cloud optical depth and reflectance are
34 clearly regime-dependent. Some cloud properties trends actually do exist only in some
35 particular regimes. Compared to observations, models underestimate cloud cover and
36 overestimate cloud optical depth and reflectance. Climate models poorly reproduce regime
37 occurrence and their evolution in time, as well as variations in cloud properties associated
38 with regime change. It means that errors in the simulation of clouds from climate models are
39 firstly due to errors in the simulation of the dynamic and thermodynamic environmental
40 conditions.

41 **1. Introduction**

42 Cloud response to anthropogenic forcing remains one of the main uncertainties for
43 model-based estimates of climate prediction evolution [Soden *et al.* 2006; Webb *et al.* 2006;
44 Ringer *et al.* 2006]. In the Tropics, the response of low level tropical clouds (below 440 hPa)
45 to anthropogenic forcing is highly variable from one climate model to another, suggesting that
46 low-level clouds contribute significantly to tropical climate cloud feedback uncertainties
47 [Bony and Dufresne 2005]. Bony *et al.* [2004] showed that tropical low-clouds have a
48 moderate sensitivity to temperature, but their statistical weight is so important that they could
49 have a large influence on the tropical radiation budget. As a consequence, it is necessary to
50 study low-level clouds in a context of global warming.

51 Tropical low clouds and their relations to dynamic and thermodynamic variables have
52 been widely studied in the past: in the Pacific Ocean [Clement *et al.* 2009. Klein *et al.* 1995.
53 Norris 1998; Norris and Klein 2000; Lau and Crane 1995; Kubar *et al.* 2010], in the Atlantic
54 Ocean [Zhang *et al.* 2009; Mauger and Norris 2010; Oreopoulos and Davis 1993], and in all
55 tropical oceans [Williams *et al.* 2003; Yuan *et al.* 2008; Klein and Hartman 1993; Sandu *et al.*
56 2010; Rozendal and Rossow 2003; Medeiros and Stevens 2009; Bony *et al.* 2004]. Only a few
57 papers are dedicated to the interannual variability of low-clouds: Clement *et al.* [2009] used
58 fifty years of low cloud observations in the Pacific Ocean and showed for example a positive
59 trend of the total cloud fraction at the end of the 90's, associated with similar trends in the
60 thermodynamical variables; Oreopoulos and Davies [1993] used cloud satellite observations
61 in two tropical oceanic locations to study the effect of temperature variations on the cloud
62 albedo, in particular its monthly variation during five years.

63 The current paper aims at characterizing the interannual variability of south-Atlantic
64 tropical clouds located in the 0°/30°S – 30°W/8°E square (Fig. 1a), under predominance of
65 subsidence air motion. We have chosen a larger region than the “Namibian” square used in

the KH93, RR03 and Zh09 studies (Tab. 1) because this area is a location of maximum stratus (KH93), and the goal of the current study is to examine all types of clouds associated with subsidence conditions. The high precipitation isolines in Fig. 1a show that the region under study is exposed to the ITCZ (Inter-Tropical Convergence Zone) in the northern edge in DJF (December – January – February), but not in JJA (June – July – August). Most of the time, this region is exposed to the descending air masses of the Hadley cell; in JJA its southern edge could be influenced by the subtropical anticyclone [Venegas *et al.* 1996]. This region contains both opaque stratocumulus clouds along the African coast, and shallow cumulus clouds westwards (Tab. 1, 3rd line). Like previous studies (RR03, Zh09 for the Atlantic Ocean; Klein *et al.* 1995; Norris 1998; Norris and Klein 2000 for equivalent subsidence locations in the Pacific Ocean), we analyze DJF and JJA independently because those are opposite seasons in terms of ITCZ influence.

The first objective of this paper is to analyze (i) the evolution of monthly mean cloud radiative properties over two decades in a region of subsidence, and (ii) the evolution of the concommittent dynamic and thermodynamic atmospheric properties. We try to determine if there is a robust relationship between these environmental variables (from reanalysis) and the observed cloud radiative properties (seasonal averaging and spatial resolution of 2.5° x 2.5°), and if this relationship is stable over two decades. It would suggest that we could know cloud radiative properties when dynamic and thermodynamic conditions are known. Moreover, our confidence in model-based predictions of future climate, depends on the ability of models to simulate realistically the current climate. The second objective of this paper is to evaluate the ability of two climate models to reproduce the evolution over two decades of (i) the observed cloud properties, (ii) the concommittent dynamic and thermodynamic atmospheric conditions, and (iii) the relationship between these environmental conditions and cloud radiative properties.

91 Cloud properties are first characterized using satellite observations (Sect. 2). Then, we
92 focus (Sect. 3) on the characterization of dynamical and thermodynamical regimes and their
93 evolution with time. Sect. 4 describes the cloud properties associated with each regime and
94 their interannual variability. In each section, the main results (i.e. interannual trends) are
95 compared with simulations from the IPSL (Institut Pierre Simon Laplace 4, Hourdin et al.
96 2012) and CNRM (Centre National de Recherches Météorologiques, Voldoire et al. 2011)
97 climate models. Discussion and conclusion are drawn in Sect. 5.

98

99 **2. Cloud satellite observations**

100 2.1. Satellite data

101 Most papers studying tropical clouds (Tab. 1) are based on satellite observations.
102 Many of those use ISCCP (International Satellite Cloud Climatology Project, *Rossow et al.*
103 1991a and b; 1993; 1996; 2004) Cloud Fraction (CF), e.g: *Clement et al.* [2009], *Klein and*
104 *Hartman* [1993], *Rozendal and Rossow* [2003], *Williams et al.* [2003], *Medeiros and Stevens*
105 [2009], *Zhang et al.* [2009], *Lau and Crane* [1995], *Oreopoulos and Davies* [1993]. A few
106 papers study tropical low clouds with A-Train observations that give more detailed
107 information on cloud properties: *Sandu et al.* [2010] used cloud types and cloud fraction from
108 MODIS (Moderate Resolution Imaging Spectroradiometer), associated with collocated
109 observations of water vapor and precipitation; *Mauger and Norris* [2010] used both MODIS
110 and CERES (Clouds and the Earth's Radiant Energy System) to study the influence of
111 previous meteorological conditions on sub-tropical cloud properties; *Kubar et al.* [2010] used
112 the more complex observations from CALIPSO (Cloud Aerosol Lidar and Infrared
113 Pathfinder) and CloudSat along a tropical cross-section during one year.

114 Here, we use three datasets to characterize clouds: cloud fractions and optical depths
115 from ISCCP D2 products [*Rossow et al.* 1991 and 1996; *Rossow and Schiffer* 1991], cloud

116 fractions from CALIPSO-GOCCP (CALIPSO – GCM Oriented CALIPSO Cloud Product,
117 *Chepfer et al.* 2010), and visible reflectance from ISCCP/Meteosat DX products [*Desormeaux*
118 *et al.* 1993].

119

120 *a) ISCCP cloud fraction and optical depth*

121 The ISCCP analyzes satellite radiance measurements to retrieve cloud fraction and
122 optical depth. The same algorithms are applied to several spaceborne instruments, such as
123 GOES (Geostationary Operational Environmental Satellite) instruments and Meteosat, or
124 polar orbiters, in order to get long-term information on clouds at global scale. We used the
125 cloud fraction for low-level clouds ($CF_{low/ISCCP}$, cloud top pressure P_{top} between ground and
126 680 hPa), mid-level clouds ($CF_{mid/ISCCP}$, P_{top} between 680 hPa and 440 hPa), and high-level
127 clouds ($CF_{high/ISCCP}$, P_{top} under 440 hPa) as well as the total cloud fraction CF_{ISCCP} (sum of CF
128 at the three pressure levels) and optical depth τ , results of the D2 data. Because cloud fraction
129 retrieval is based on passive remote-sensing measurements, there is no overlap between
130 $CF_{low/ISCCP}$, $CF_{mid/ISCCP}$ and $CF_{high/ISCCP}$, hence CF_{ISCCP} never exceeds 100%.

131 We analyzed 23 years (1984 to 2006) of monthly-mean data averaged seasonally (in
132 DJF and JJA) and spatially at a horizontal resolution of $2.5^\circ \times 2.5^\circ$. These observations are
133 averaged over the diurnal cycle, unlike the observations used hereafter.

134

135 *b) CALIPSO-GOCCP cloud fraction and vertical profile*

136 The CALIPSO satellite, launched in 2006, holds the lidar CALIOP (Cloud-Aerosol
137 Lidar with Orthogonal Polarization), which allows the characterization of the cloud vertical
138 structure. The CALIPSO-GOCCP [*Chepfer et al.* 2010] was initially designed to evaluate
139 cloudiness in Global Circulation Models. It is derived from CALIPSO Level 1 NASA
140 (National Aeronautics and Space Administration) products [*Winker et al.* 2009] and contains

141 four types of files, including seasonal cloud fraction maps at three levels of altitude (low-,
142 mid-, and high-level defined consistently with ISCCP). As this retrieval is based on active
143 remote sensing, there can be an overlap between the low-level cloud fraction ($CF_{low/GOCCP}$),
144 the mid-level one ($CF_{mid/GOCCP}$), and the high-level one ($CF_{high/GOCCP}$); and the sum of the
145 three can be larger than 100%. Nevertheless, the total cloud fraction CF_{GOCCP} detects if there
146 is a cloud in the column (it does not correspond to the sum of the low, mid and high cloud
147 fraction) and cannot exceed 100%. We also used vertical profiles of cloud fraction
148 ($CF_{GOCCP3D}$) at 40 equidistant levels (480m) from the ground to 20 km of altitude.

149 We analyzed four years (2007 to 2010) of CALIPSO-GOCCP seasonal mean (DJF and
150 JJA) cloud fractions. Initially, the CALIPSO-GOCCP cloud detection is done at the full
151 CALIOP Level 1 horizontal resolution (330 m along track and 75 m across track) to allow the
152 detection of small-size fractionated boundary layer clouds; cloud occurrences are then
153 statistically summarized over $2.5^\circ \times 2.5^\circ$ grid box consistently with ISCCP cloud fraction.
154 The CALIPSO-GOCCP cloud fraction reported here are collected in day-time (1330 LST, A-
155 train orbit). In the current study, this product helps to understand the vertical distribution of
156 clouds from one season to another, and from one regime to another, but is not used to draw
157 any trend.

158

159 *c) ISCCP/Meteosat visible reflectance*

160 To consolidate our analysis, and avoid making it dependent of the inversion
161 algorithms, we also use Meteosat Level 1 reflectance measurements (visible, wavelength near
162 0.6 μm) from ISCCP/Meteosat DX files. Reflectance can be seen as a proxy of cloud fraction
163 combined to cloud optical depth: a radiative signature of the cloud scene.

164 Since we focus on a given geographical zone, the satellite viewing direction is
165 constant; moreover the analysis is not impacted by the change of instruments as shown by

166 clear sky evolution in Appendix A. We use reflectance observed at a constant time 1200 UTC
167 (3-hours time slot, as close as possible to the CALIPSO overpass time), seasonally averaged
168 (DJF and JJA) during 23 years. The horizontal resolution is $0.5^\circ \times 0.5^\circ$, and the reflectance
169 uncertainty is 0.004. Since the satellite azimuthal relative angle changes with the season, DJF
170 and JJA reflectance cannot be compared in a quantitative way. Nevertheless, as the angles are
171 the same every year at the same date and same location, the same seasons can be compared
172 over different years, in order to study the interannual variability (Appendix A). Typically,
173 stratus (St) are associated with higher reflectance than stratocumulus (Sc), cumulus (Cu)
174 being the less reflective.

175

176 2.2. Cloud properties observed by satellite in the region under study: main patterns

177

178 *a) Spatial distribution*

179 Reflectance value is high in three regions (Fig. 1i-j): northeast, southwest and mid-
180 east, all with low standard deviations suggesting homogeneity of cloud solar reflectivity over
181 years. This is consistent with previous studies that found a lot of stratus in this area, even if
182 the area of maximum reflectance is not completely contained in the Namibian square studied
183 previously (KH93, RR03, Zh09).

184 The mid-east region is characterized by important cloud fractions (about 0.8) observed
185 by both GOCCP (Fig. 1b-c) and ISCCP (Fig. 1e-f) with low standard deviations (not shown),
186 and large optical thickness ($\tau \sim 8$, Fig. 1g) with important standard deviations (not shown).
187 This suggests that low clouds are present most of the time in this region but their cloud optical
188 thickness is highly variable (probably due to transitions between different types of low
189 clouds). This region corresponds with the “Namibian” area studied in KH93 who show that
190 stratus clouds are more frequent in JJA than in DJF (0.67 versus 0.6): opposite result is found

191 for CF_{ISCCP} (Fig. e versus Fig. 1f) probably due to the large amount of clouds at higher levels
192 (Fig. 1d).

193 The southwest region shows large cloud fraction (about 0.8) in ISCCP and GOCCP
194 with smaller values of optical thickness ($\tau \sim 4$, Fig. 1i-j). Examining maps for low-/mid-/high-
195 cloud fractions from ISCCP and GOCCP (not shown) indicates that this southwest region is
196 mostly characterized by a mix of mid- and high-clouds.

197

198 *b) Mean cloud properties*

199 When averaged in time over 23 years and spatially over the entire area under study,
200 cloud covers (Tab. 2) show that ISCCP detects almost only low-clouds (about 40%) whereas
201 GOCCP detects some mid- and high-clouds (up to 20%). In complement, the mean vertical
202 profile (Fig. 1d) shows that high-clouds are often present in this area ($CF_{GOCCP3D} \sim 20\%$),
203 with a maxima around 12 km of altitude, and these high clouds are not optically thin enough
204 to mask the important presence of low clouds.

205 The two seasons exhibit similar cloud covers, but the small seasonal variation (less
206 than 10% difference) is different in ISCCP and CALIPSO-GOCCP. The ISCCP cloud
207 fraction CF_{ISCCP} and optical depth τ are slightly higher in DJF than in JJA (Tab. 2). This is
208 still the case when considering each year individually (not shown). The seasonal variation
209 from GOCCP is opposite to ISCCP: the mean cloud cover is slightly higher in JJA than in
210 DJF (Tab. 2, Fig. 1b-c-e-f). The discrepancy between ISCCP and GOCCP occurs only in JJA
211 in which GOCCP observes more clouds than ISCCP at all levels of altitudes. The important
212 result is that the difference between the cloud covers from the two datasets is less than 10%
213 for all levels of altitude: both datasets will be used together for the rest of the interpretation.

214 The detailed cloud vertical distribution (Fig. 1d) changes with season: JJA shows less
215 high clouds and more low clouds ($CF_{GOCCP3D} \sim 0.25$) than DJF. The low cloud variation can

216 be due in part to the high cloud masking low clouds in DJF. These seasonal differences in the
217 vertical cloud distribution confirm that the cloud types are different during each season in the
218 area under study, and that the two seasons need to be analyzed independently in the rest of
219 this paper (even when split into regime).

220 The results of climate models simulations obtained by the IPSL and CNRM models in
221 the same region and period are given in Tab. 2. Those results have been obtained with the
222 ISCCP [Webb and Klein 2006], CALIPSO [Chepfer et al. 2008] and reflectance simulators
223 [Konsta et al., under review] included in COSP (CFMIP Observations Satellites Package,
224 Bodas et al. 2011). This way, “Climate Model+Simulator” (CMS) outputs are kept consistent
225 with satellite observations. In this region and on average over 23 years, both CMS
226 underestimate by a factor of two the cloud cover whatever the season (Tab. 2), and
227 overestimate significantly the reflectance (up to + 0.1 in JJA), confirming that 1) climate
228 models do not produce enough clouds in the tropics (particularly at low levels), and 2) when
229 models do create clouds, they are optically too thick. This result is consistent with the “too
230 few, too bright” low-level tropical cloud problem identified in CMIP5 models (i.e. Nam et al.
231 2012).

232

233 2.3. Interannual variability of cloud properties (1984-2006)

234 The interannual variability of cloud fraction CF_{ISCCP} , optical depth τ and reflectance
235 ref is large over 23 years (Fig. 2) in both DJF and JJA. The trend of each variable, i.e. the
236 value of the linear regression slope multiplied by the number of years is given in each subtitle
237 in Fig. 2 (it is outlined within a rectangle when it is superior to the value of the standard
238 deviation). In DJF, the cloud optical depth τ and reflectance ref have increased in 23 years,
239 despite almost no change in the cloud cover CF_{ISCCP} . In JJA, the cloud optical depth has
240 increased of +1.2 in 23 years and reflectance remains almost stable. Anomalies can be

241 isolated: for example, reflectance is enhanced by +0.3 in DJF 1997 and JJA 1985, there is a
242 strong deficit of *ref* and τ in DJF 1988. Year 1997 corresponds with an El Niño event: the
243 important anomalies of cloud properties for this year are consistent with *Belon et al.* [2010]
244 results: in the tropics, the fraction of interannual variability of low-cloud cover that is related
245 to SST variability is driven by El Niño index.

246 This important variability in observations is well reproduced by CNRM model,
247 whereas it is smoother with IPSL model (Fig. 2d-e-f). The two models give very different
248 results: they do not show the same years of maximum and minimum for example. For one
249 single model, DJF and JJA are in phase (increase or decrease the same years, maximum and
250 minimum the same years...) whereas it is not the case in observations.

251

252 **3. Characterization of the atmospheric circulation in the region under study**

253 At first order, the cloud occurrences and optical depth depend on the atmospheric
254 circulation of the air masses; as a consequence, any change in the atmospheric circulation will
255 affect cloud properties. In order to understand if the observed interannual variability of the
256 cloud properties (and its anomalies) is mainly due to variations of atmospheric circulation or
257 to the change in cloud physical processes we will separate the cloud population in
258 atmospheric circulation regimes, based on the analysis of dynamic and thermodynamic
259 variables: in the following, it will be only called “regime”.

260

261 3.1. Definition of the regimes used in this study.

262 Various dynamic and thermodynamic variables are used in the literature to
263 characterize the atmospheric environment in the Tropics. *Bony et al.* [2004] showed that
264 clouds, and in particular low clouds, are sensitive to both large-scale circulation and
265 thermodynamic structure of the atmosphere. *Klein et al.* [1995] also concluded that the low-

level cloud fraction is better correlated to temperatures 24 to 28 hours previously, than to simultaneous ones, and that this cloud fraction is linked to atmospheric circulation at the interannual scale. The Sea Surface Temperature (SST), the Lower Tropospheric Stability (LTS) and the vertical velocity of air at 500 hPa (w_{500}) are also frequently used to characterize the dynamic and thermodynamic state of the atmosphere. Wi03 showed that the clouds response depends more on changes in both w_{500} and SST than on changes in SST alone. Medeiros and Stevens [2009] suggested that w_{500} alone is not good to separate low clouds, but is useful with LTS: w_{500} identifies subsidence and LTS separates cloud types in these subsidence motions. More generally, several approaches have been followed, using only w_{500} as in Bony *et al.* [2004], only LTS as in Wyant *et al.* [2009], or a combination of both as in Medeiros and Stevens [2009]. In this study, we privileged the two w_{500} variable for the large-scale dynamics, and SST variable for the thermodynamics in the following, the combination of these two variables will be called “environmental variables”.

Figures 3 shows the distribution of SSTs and w_{500} over the region, as simulated by NCEP (National Centers for Environmental Prediction, Fig.3a-b) and ERA-Interim (ECMWF Re-Analyses, Fig 3.c-d) reanalyses, and IPSL (Fig. 3g-h) and CNRM (Fig. 3i-j) climate models. The seasonal variation of SST and w_{500} is roughly consistent with the position of the Hadley cell in the four models: the SST is colder in JJA than in DJF, and air masses ascending more ($w_{500} < 0$) in DJF than JJA. Reanalyses show higher variability than climate models, suggesting than the latter reproduce the mean values for the SST (but not for w_{500}), whereas the real variability is poor for models. In JJA for example, strong subsidence is too frequent and weak subsidence is missing for CNRM model, and strong subsidence never appears for IPSL model.

The PDF (Probability Density Function) of w_{500} and SST from NCEP (not shown) have been examined and values are split following sections of the curves. It leads the

291 separations of the dataset in five regimes (white lines in Fig.3) that are studied independently
292 hereafter: an ascending regime (“As”) associated with deep convection, strong subsidence
293 with cold (“SSu-cold”) or warm (“SSu-warm”) SSTs (associated with Stratocumulus), and
294 weak subsidence with cold (“WSu-cold”) or warm (“WSu-warm”) SSTs associated with
295 trade-wind cumulus). Weak and strong subsidence are separated at 30 hPa/day, and warm and
296 cold SSTs are separated at 298,5 K (respectively 296,5 K) in DJF (respectively JJA).

297

298 3.2. Interannual variability of regime distribution (1984-2010)

299 The occurrence of each regime evolves in time over 27 years (1984 to 2010, in order
300 to get both ISCCP years and GOCCP years). Figure 4 presents the interannual evolution of
301 their occurrence as an anomaly. The interannual trends (calculated as in Sect. 2.3) that are
302 statistically significant (underlined by a rectangle in the subtitle of each subplot in Fig.4),
303 represent about half (11 out of the 20) of the values reported here. A single regime in one
304 season exhibits a consistent interannual trend statistically robust in both datasets (NCEP and
305 ERA-Interim): the occurrence of the As regime decreases by 12-15% in 27 years in DJF. For
306 all other regimes, the trends obtained with the two reanalyses are inconsistent and/or not
307 statistically representative. Moreover, based in NCEP reanalyzes, the As regime is dominant
308 in DJF from 1984 to 1990 whereas SSu-cold dominates 1998 to 2010 (not shown).

309 Similarly to the reanalyses, climate models (Fig. 4f and g) do not suggest a significant
310 change in regime occurrence with time, except for the WSu-warm regime in DJF (only for
311 CNRM model). Nevertheless, this regime becomes more frequent with time in DJF for
312 CNRM model, which is in contradiction with the trend produced by ERA-Interim and NCEP
313 reanalyses. Moreover, trends that are significant in the reanalyses are not significant in the
314 models.

315 This suggests that both climate models are far of reproducing the occurrence of
316 regimes given by the reanalyses, but they are even more far away of reproducing their
317 evolution in time. In particular, the models predict that ascending branch of the Hadley cell
318 (As regime) is more frequent, which is not the case in the reanalyses.

319

320 **4. Analysis of cloud properties for each regime**

321 4.1. Characterization of cloud properties in regimes

322 To assess how robust is the mean cloud properties dependence on the regime, results
323 obtained with the different satellite datasets (ISCCP, CALIPSO-GOCCP) and reanalyses
324 datasets (NCEP and ERA-Interim) are reported in Fig. 5.

325 Observations (blue and green) are consistent for both datasets: the mean cloud fraction
326 varies slightly (between 0.4 and 0.6) when the regime changes, whereas the mean optical
327 depth (between 3 and 6) and the mean reflectance (between 0.15 and 0.25) are significantly
328 regime dependent, and seasonally dependent. In DJF, the larger optical depth and reflectance
329 are associated with strong subsidence regime (stratocumulus), which optical depth decreases
330 significantly in winter. In JJA, the cloud cover is about the same for all regimes, but larger
331 optical depths (and reflectance) are encountered in deep convection (As regime). These results
332 show that regimes do not drive significantly the mean cloud cover in the region, but do drive
333 the mean cloud optical depth and reflectance, and significantly the vertical structure (Fig. 6).
334 In particular, for the subsidence regime, the SST impacts more the vertical structure than w_{500} ,
335 consistently with Wi03 results, in particular in winter (JJA). However, a regime (as defined in
336 this study) does not by itself completely determine the cloud optical depth and reflectance: for
337 a given regime the mean optical depth and reflectance also depend on the season. This
338 seasonal dependency can be explained by the change in the cloud vertical distribution as
339 shown in Fig. 6.

340 Compared to the observations, CMS underestimate the cloud cover (Fig. 5a and d) by
341 a factor of two (or more) in all regimes and seasons, except in the As regime that is better
342 described by one CMS (CNRM). Differences between observations and CMS cloud cover can
343 be more than a factor of three for some regimes: SSu-cold and -warm (but they are not
344 significant in term of population, Fig.3) and WSu-cold in DJF, and SSu-warm in JJA (i.e.
345 41% of the population for CNRM model, Fig. 3h). It confirms that the boundary layer cloud
346 scheme, that drives the amount of cloud forms in subsidence conditions, remains a
347 challenging task for those two climate models.

348 The IPSL model errors on the reflectance (overestimate, Fig. 5c-f) and on the cloud
349 cover (underestimate, Fig. 5a-c) likely compensate to produce correct shortwave fluxes at the
350 top of the atmosphere (in both seasons) as already mentioned in previous section. Figure 5
351 shows that this error compensation applies to all regimes that are significant in term of
352 population.

353

354 4.2. Interannual variability of cloud properties using regime classification

355 Figure 7 shows the trends of observed cloud variables (blue and green bars) over 23
356 years in each regime. It means for example that *ref* has an increase of +0.03 in 23 years for
357 the As regime in DJF (based on NCEP reanalyses). The cloud fraction is stable in time in all
358 regimes (contrary to Clement et al. 2009), except in the warm strong subsidence regime where
359 it decreases (Fig. 7a) consistently with the reflectance (Fig. 7c). In the other four regimes,
360 cloud optical depth (Fig. 7b) and reflectance (Fig. 7c) have increased very slightly in summer
361 (DJF) over 23 years (about +0.5 for τ and about +0.035 for *ref*, in 23 years). A more
362 important increase of cloud optical depth occurs in winter (JJA) in all regimes (about +1.5),
363 but it is not associated with change in the reflectance that remains stable in time.

364 A trend is robust if it is observed in both sets of reanalyses, hence the final results are:
365 (1) a decrease of cloud fraction for the SSu-warm regime in DJF, (2) an increase of optical
366 depth for weak subsidence in DJF and for all regimes (except ascent) in JJA, and (3) an
367 increase of reflectance in the ascent regime in DJF.

368 In most of the cases, the IPSL CMS does not show any robust trend in the cloud cover
369 and reflectance. When it shows some trends (vertical arrows in Fig. 7), those are sometimes in
370 contradiction with the observations: in the WSu-warm regime, the modelled *CF* and *ref* in
371 JJA increase in time along the last 23 years (Fig. 7c) which is not consistent with the
372 observations. This increase of *ref* suggests that the clouds of this specific regime reflect more
373 solar light now than 23 years ago. But the observations disagree with this modelled
374 reflectance trend.

375

376 **5. Conclusion**

377 We have examined cloud properties in a tropical subsidence area (south Atlantic
378 Ocean) using 23 years of ISCCP cloud fractions and optical depths, complemented with 23
379 years of visible reflectance from ISCCP/Meteosat, and cloud vertical profiles from
380 CALIPSO-GOCCP collected during four years. We first studied the mean cloud properties
381 (cloud cover, optical depth, and reflectance) in DJF and JJA. The region under study contains
382 about 40% of low-level clouds and 20% of high-clouds (around 12 km). The difference
383 between ISCCP and GOCCP cloud cover is less than 10%, but the small seasonal variation is
384 not consistent between the two dataset. Then we looked at the interannual variability of cloud
385 properties over 23 years using ISCCP: cloud cover is stable in time and cloud optical depth
386 exhibits a positive trend (+0.55 in DJF and +1.2 in JJA).

387 We compared the observational results with output from climate models (IPSL and
388 CNRM models within CMIP5), coupled with COSP to ensure that differences can be

389 attributed to model defects. Models underestimate cloud cover by a factor of two, and
390 overestimate reflectance (+0.1). The CNRM model produces a stable cloud cover in time, in
391 agreement with observations, whereas the IPSL model shows a significant and unrealistic
392 positive cloud cover trend over the years.

393 As the cloud formation and properties are primarily driven by atmospheric dynamic
394 and thermodynamic variables, we examined the regimes (characterized with the SST and w_{500}
395 from NCEP and ERA-Interim) that dominate DJF and JJA. We classified atmospheric
396 situations in five categories: ascending air masses, moderate subsidence with warm / cold
397 SSTs, strong subsidence with warm / cold SSTs. The occurrence of each regime in the region
398 depends significantly on the dataset used (NCEP or ERA-Interim). The evolution in time of
399 the occurrence of each regime along the 23 years is different and inconsistent in both datasets,
400 except for the “ascending air” regime: its occurrence decreases significantly in time (of more
401 than 10%) according to both datasets. The occurrence of all regimes is poorly reproduced by
402 both climate models (CNRM and IPSL). Moreover, both report an increase in occurrence of
403 the “ascending air” regime contrarily to the observations.

404 We examined the relationship between environmental variables and the observed
405 cloud properties (seasonal averaging and spatial resolution of $2.5^\circ \times 2.5^\circ$). Observations
406 indicate that the cloud cover (0.4 to 0.6) is slightly regime dependent whereas the optical
407 depth (4 to 6) and the reflectance (0.15 to 0.25) are more significantly regime dependent.
408 Differences between modeled and observed cloud cover and reflectance are not regime
409 dependent.

410 We study the evolution of the relationship between the environmental variables and
411 cloud radiative properties over two decades. The observations exhibit two robust trends over
412 23 years in specific regimes. The optical depth increases only in weak subsidence conditions
413 in DJF (+0.6), and for weak and strong subsidence regimes in JJA (+1). The reflectance

414 increases only for the ascent regime in DJF (+0.03). This later trend is reproduced by IPSL
415 model with a smaller amplitude (+0.01). Trends detected in cloud properties before the
416 regime separation are now explained in some regime, particularly in DJF: the decrease of
417 cloud fraction over 23 years is explained by only one regime (strong subsidence with warm
418 SSTs), as for the optical depth increase which is detected only for weak subsidence, whereas
419 the reflectance increase is not detected in the subsidence (only in ascent).

420 In summary, this study suggests that the main difficulty to built reliable relationships
421 between environmental variables and clouds comes from the significant uncertainties in these
422 environmental variables produced by the different reanalyses and by climate models. It limits
423 the ability to detect robust regime-dependent trend in the observations, and it may be the first-
424 order limitation for models to reproduce observed clouds.

425 Future work will consist in extending this study to the entire tropical belt including all
426 CMIP5 models and the same two sets of reanalyses. It will aim at determining if, at this scale,
427 some of the regimes (and related trends) are better reproduced than others and in these cases if
428 the link between cloud properties and environmental variable (and related trends) is better
429 predicted by models.

430

431

432 **Appendix A**

433 There are two well-known problems for the retrieval of cloud fraction using satellite
434 passive remote sensing, in particular from the ISCCP program: the variations of the satellite
435 angles, and the calibration of satellites when the instruments are changed. In this Annex we
436 investigate if these problems affect the dataset used in our study.

437 Figure A1.a shows an example of the satellite viewing angle θ_v for the complete area
438 of study, for one day of the database. The values of this angle are between a few degrees and
439 approximately 40° , depending on the location. Figure A1.b shows the percentage of days
440 when θ_v is lower or smaller than its median value by more than 2° , for each pixel during the
441 time period of the study. This percentage is always lower than 4%, and Fig. A1.c shows that
442 the concerned θ_v do not deviate from the median by more than 3° . This shows that, during the
443 23 years of the study, the variations of θ_v are so small that they should not be a problem for
444 our study of reflectance trends.

445 Figure A2.a is the same as Fig. A1.a but for the satellite relative azimuthal angle ϕ .
446 The values of this angle are between 0° and 180° , depending on location and time. Figure
447 A2.b is approximately the same as Fig. A1.b but for each pixel, the percentage is calculated
448 every year for the same day, so from 23 values, in order to remove the natural variations of ϕ
449 and only consider the variations due to technical problems. Another difference is that the
450 percentage is calculated when ϕ is lower or smaller than its median value by more than 5° .
451 This percentage is about 4% or 8% (one or two cases on twenty three) and Fig. A2.c shows
452 that the concerning ϕ can be different from the median value by 50° . Figure A3 shows the
453 value of the solar angle for the area under study, in January (Fig. A3a) and in July (Fig. A3b).
454 Using extreme values of these three angles (Fig. A1-A3), the correspondence between
455 reflectance and optical depth values has been calculated. The calculation is done using a
456 doubling/adding radiative transfer code [De Haan et al. 1987], assuming the atmosphere is

457 plane parallel infinite. The atmosphere contains a cloud composed of liquid water spherical
458 particles of 6- μm radius (Mie Theory). Six values of cloud optical depth ($\tau_{calc} = 0, 1, 5, 10,$
459 $50, 100$) are considered and four different geometries (two extremes of January, and two
460 extremes of July). Figure A4 is an illustration of this calculation (using a linear interpolation),
461 and it shows that for one given optical depth, the reflectance variability is very small from one
462 geometry to another (less than 0.1).

463 Figure A5 shows the variation in time of the clear sky reflectance for the complete
464 time period by selecting, for each day, the smallest reflectance in the area. The figure shows
465 that instrument changes are not associated with any gap in clear sky reflectance values. It
466 follows that instrument changes are not either a problem for the current study that focuses on
467 reflectance.

468

469

470 **Acknowledgments**

471 The ISCCP DX data were obtained from the International Satellite Cloud Climatology
472 Project data archives at NOAA/NESDIS/NCDC Satellite Services Group,
473 ncdc.satorder@noaa.gov, on January, 2005. Thanks are also due to the Climserv team for the
474 computing facilities and the data availability. Also thanks to Vincent Noël for internal review.
475 Thanks are due to the reviewers for the very interesting suggestions: it has help for changing
476 and improving the study.

477

478 **References**

- 479
480 Bellon G., G. Gastineau, A. Ribes, and H. Le Treut, 2011: Analysis of the variability
481 of the tropical climate in a two-column framework, *Clim. Dyn.*, DOI 10.1007/s00382-010-0864-
482 5
- 483 Bony S. and J-L Dufresne, 2005: Marine boundary layer clouds at the heart of cloud
484 feedback uncertainties in climate models. *Geophys. Res. Lett.*, **32**, No. 20, L20806, doi:
485 10.1029/2005GL023851.
- 486 Bony S., J.-L. Dufresne, H. L. Treut, J.-J. Morcrette and C. Senior, 2004: On dynamic
487 and thermodynamic components of cloud changes. *Clim. Dyn.*, **22**, 71-86.
- 488 Chepfer H., S. Bony, D. Winker, G. Cesana, J. L. Dufresne, P. Minnis, C. J.
489 Stubenrauch and S. Zeng, 2010: The GCM-Oriented CALIPSO Cloud Product (CALIPSO-
490 GOCCP). *J. Geophys. Res.*, **115**, D00H16, doi:10.1029/2009JD012251.
- 491 Clement A. C., R. Burgman, J. R. Norris 2009: Observational and Model Evidence for
492 Positive Low-Level Cloud Feedback. *Science*, **325(5939)**, 460-464.
- 493 Desormeaux, Y., W.B. Rossow, C.L. Brest, and G.G. Campbell, 1993: Normalization
494 and calibration of geostationary satellite radiances for the International Satellite Cloud
495 Climatology Project. *J. Atmos. Oceanic Tech.*, **10**, 304-325.
- 496 Hourdin, F., J.-Y. Grandpeix, C. Rio, S. Bony, A. Jam, F. Cheruy, N. Rochetin, L.
497 Fairhead, A. Idelkadi, I. Musat, J.-L. Dufresne, A. Lahellec, M.-P. Lefebvre, and R. Roehrig,
498 2012 : LMDZ5B: the atmospheric component of the IPSL climate model with revisited
499 parameterizations for clouds and convection, *Clim. Dyn.*, **79**, doi:10.1007/s00382-012-1343-y
- 500 Klein S. A. and D. L. Hartmann 1993: The seasonal cycle of low stratiform clouds. *J.*
501 *Climate*. **6(8)**, 1587-1606.

- 502 Klein S. A., D. L. Hartmann, J. R. Norris, 1995: On the Relationships among Low-
503 Cloud Structure, Sea-Surface Temperature, and Atmospheric Circulation in the Summertime
504 Northeast Pacific. *Journal of Climate*, **8(5)**, 1140-1155.
- 505 Konsta D., JL. Dufresne, H. Chepfer, A. Idelkali, G. Cesana, 2012: Evaluation of
506 clouds simulated by the LMDZ5 GCM using A-train satellite observations (CALIPSO-
507 PARASOL-CERES), *Clim. Dyn.*, under review
- 508 Kubat T. L., D. E. Waliser, and J.-L. Li, 2010: Boundary layer and cloud structure
509 controls on tropical low cloud cover using A-Train satellite data and ECMWF Analyses. *J.*
510 *Climate*, **24**, doi: 10.1175/2010JCLI3702.1.
- 511 Lau N. C. and M. W. Crane 1995: A Satellite View of the Synoptic-Scale
512 Organization of Cloud Properties in Midlatitude and Tropical Circulation Systems. *Monthly*
513 *Weather Review*, **123(7)**, 1984-2006.
- 514 Mauger G. S. and J. R. Norris 2010: Assessing the Impact of Meteorological History
515 on Subtropical Cloud Fraction. *J. Climate*, **23(11)**, 2926-2940.
- 516 B. Medeiros and B. Stevens, 2009: Revealing differences in GCM representations of
517 low clouds, *Clim. Dyn.*, **36**, 385 – 399.
- 518 Nam C., S. Bony, JL Dufresne, H. Chepfer, 2012: The 'too few, too bright' tropical
519 low-cloud problem in CMIP5 models, *Geophys. Res. Lett.*, idoi:10.1029/2012GL053421.
- 520 Norris J. R., 1998: Low cloud type over the ocean from surface observations. I.
521 Relationship to surface meteorology and the vertical distribution of temperature and moisture.
522 *Journal of Climate*, **11(3)**, 369-382.
- 523 Norris J. R. and S. A. Klein 2000: Low cloud type over the ocean from surface
524 observations. Part III: Relationship to vertical motion and regional surface synoptic
525 environment. *J. Climate*, **13(1)**, 245-256.

- 526 Oreopoulos L. and R. Davies, 1993: Statistical dependence of albedo and cloud cover
527 on sea surface temperature for two tropical marine stratocumulus regions. *J. Climate*, **6**, 2434-
528 2447.
- 529 Ringer, M.A. et al., 2006. Global mean cloud feedbacks in idealized climate change
530 experiments. *Geophys. Res. Lett.*, **33**(7), L07718.
- 531 Rossow W. B. and R. A. Schiffer, 1991: ISCCP cloud data products. *Bull. Amer.*
532 *Meteor. Soc.*, **72**, 2–20.
- 533 Rossow W. B., L. C. Garder, P. J. Lu, and A. W. Walker, 1991: International Satellite
534 Cloud Climatology Project (ISCCP), documentation of cloud data. WMO/TD-266 (revised),
535 World Climate Research Programme (ICSU and WMO), Geneva, Switzerland, 76 pp. plus 3
536 appendixes.
- 537 Rossow W. B., A. W. Walker, and L. C. Garder, 1993: Comparison of ISCCP and
538 other cloud amounts. *J. of Climate*, **6**, 2394–2418.
- 539 Rossow W. B., D. E. Beuschel, and M. D. Roiter, 1996: International Satellite Cloud
540 Climatology Project (ISCCP) documentation of new cloud datasets. WMO/TD-737, World
541 Climate Research Programme (ICSU and WMO), Geneva, Switzerland, 115 pp.
- 542 Rossow W.B. and E. Duenas, 2004: The International Satellite Cloud Climatology
543 Project (ISCCP) web site: An online resource for research. *Bull. Amer. Meteorol. Soc.*, **85**,
544 167-172.
- 545 Rozendaal, M.A., and W.B. Rossow, 2003: Characterizing some of the influences of
546 the general circulation on subtropical marine boundary layer clouds. *J. Atmos. Sci.*, **60**, 711-
547 728.
- 548 Sandu I., B. Stevens, and R. Pincus, 2010: On the transitions in marine boundary layer
549 cloudiness. *Atmospheric Chemistry and Physics*, **10**(5), 2377-2391.

- 550 Soden, B.J., and I.M. Held, 2006: An assessment of climate feedbacks in coupled
551 ocean-atmosphere models. *Journal of Climate*, **19(14)**, 3354-3360.
- 552 Venegas S. A., L. A. Mysak, and D. N. Straub, 1996. Evidence for interannual and
553 interdecadal climate variability in the south atlantic. *Geophys. Res. Lett.*, **23(19)**, 2673-2676.
- 554 Volodire A., E. Sanchez-Gomez, D. Salas y Méria, B. Decharme, C. Cassou, S.
555 Sénési, S. Valcke, I. Beau, A. Alias, M. Chevallier, M. Déqué, J. Deshayes, H. Douville, E.
556 Fernandez, G. Madec, E. Maisonnave, M.-P. Moine, S. Planton, D. Saint-Martin, S. Szopa, S.
557 Tyteca, R. Alkama, S. Belamari, A. Braun, L. Coquart, F. Chauvin, 2011: The CNRM-CM5.1
558 global climate model: description and basic evaluation, *Clim. Dyn.*, accepted,
559 DOI:10.1007/s00382-011-1259-y
- 560 Webb, M.J. et al., 2006: On the contribution of local feedback mechanisms to the
561 range of climate sensitivity in two GCM ensembles. *Climate Dynamics*, **27**, 17-38.
- 562 Williams K. D., M. A. Ringer, and C. A. Senior, 2003: Evaluating the cloud response
563 to climate change and current climate variability. *Climate Dynamics*, **20**, 705-721.
- 564 Winker D. M., M. A. Vaughan, A. Omar, Y. X. Hu and K. A. Powell, 2009: Overview
565 of the CALIPSO mission and CALIOP data processing algorithms. *J. Atmos. Ocean. Tech.* **26**
566 2310-2323.
- 567 Wyant M., C. Bretherton, and P. Blossey, 2009: Subtropical low cloud response to a
568 warmer climate in an superparameterized climate model: Part I. Regime sorting and physical
569 mechanisms. *Journal of Advances in Modeling Earth Systems*, **0(0)**.
- 570 Yuan, J. and D. L. Hartmann, 2008: Spatial and Temporal Dependence of Clouds and
571 their Radiative Impacts on the Large-scale Vertical Velocity Profile. *J. Geophys. Res.*,
572 **113**(D19201): doi:10.1029/2007JD009722.
- 573 Zhang Y. Y., B. Stevens, B. Medeiros, M. Ghil, 2009: Low-Cloud Fraction, Lower-
574 Tropospheric Stability, and Large-Scale Divergence. *J. Climate*, **22(18)**, 4827-4844.

575 **List of Tables**

576 **Table 1:** Review of previous studies concerning tropical low clouds and their relations
577 to dynamic and thermodynamic variables, when the area of study includes part of total of the
578 location of the following paper, called A. *SON is for September to November, MAM is for
579 March to May, MJJAS is for May to September, NDJFM is for November to March; **Cloud
580 Top Pressure; ***Sc for Stratocumulus, Cu for Cumulus.

581 **Table 2:** Mean values (0° - 30° S, 30° W – 8° E) of the entire database for ISCCP (1984
582 – 2006) and CALIPSO-GOCCP (2007 – 2010). Equivalent simulated values from the IPSL
583 and CNRM models have been added when available.

584

585

586

Reference	Important results in the A area	Location
<i>Klein and Hartman 1993 [KH93]</i>	- SON* is season of maximum stratus & maximum LTS - A is an area of maximum stratus - interannual variability in stratus are related to changes in LTS	Area contained in A
<i>Rozendal and Rossow 2003 [RR03]</i>	- $CF_{low}(MJAS^*) > CF_{low}(NDJFM^*)$ - notable differences between the low cloud areas in Pacific and the low cloud areas in Atlantic ($CF, \tau, CTP^{**} \dots$) - more the subsidence is important, more the cloud top is low	Area contained in A
<i>Sandu et al. 2010 [Sa10]</i>	- transition of decrease CF associated with strong increase of SST & decrease of LTS, & free troposphere gradual humidification - Sc to Cu*** transition is stable from one Ocean to another, but Sc CF is higher in South Hemisphere Oceans	All Atlantic Ocean
<i>Williams et al. 2003 [Wi03]</i>	- cloud response depends more on w_{500} & SST changes than on SST changes only - low clouds: many with medium τ , CF more important for strong subsidence and cold SSTs	All tropical oceans
<i>Medeiros and Stevens 2009 [MS09]</i>	- CF_{low} increase as LTS increase but is independent of w_{500} - the peak of CF_{low} is about 30%, very large and very low values of CF_{low} are rare - in A: a few shallow-Cu at high level, a lot of Sc at low level	All tropical oceans
<i>Zhang et al. 2009 [Zh09]</i>	- CF_{low} increases linearly as a function of LTS - CF_{low} & LTS: both are maximum in SON* and minimum in MAM*	Area contained in A
<i>Oreopoulos and Davies 1993 [OD93]</i>	- SST has negative correlation with Albedo and CF, also for interannual variations	Area contained in A
<i>Bony et al. 2004 [Bo04]</i>	- low clouds have moderate sensitivity to temperature change but have an important statistical weight, so a large influence on the tropical Radiative budget - cloud Radiative forcing is high for ascendance and small for subsidence	All tropical oceans

589 *Table 1: Review of previous studies concerning tropical low clouds and their relations to*
 590 *dynamic and thermodynamic variables, when the area of study includes part of total of the*
 591 *location of the following paper, called A. *SON is for September to November, MAM is for*
 592 *March to May, MJAS is for May to September, NDJFM is for November to March; **Cloud*
 593 *Top Pressure; ***Sc for Stratocumulus, Cu for Cumulus.*

595

	CF_{ISCCP}		τ_{ISCCP}		CF_{GOCCP}		<i>ref</i>	
	DJF	JJA	DJF	JJA	DJF	JJA	DJF	JJA
Low – obs	0.46	0.39	–	–	0.39	0.47	–	–
Mid – obs	0.05	0.07	–	–	0.13	0.11	–	–
High – obs	0.01	0.03	–	–	0.20	0.16	–	–
Tot – obs	0.52	0.49	4.21	3.97	0.52	0.56	0.18	0.15
Tot – mod IPSL	0.18	0.17	–	–	0.21	0.20	0.2	0.3
Tot – mod CNRM	0.22	0.21	–	–	0.26	0.26	–	–

596

597 *Table 2: Mean values (0° - $30^\circ S$, $30^\circ W$ – $8^\circ E$) of the entire database for ISCCP (1984 – 2006)*
 598 *and CALIPSO-GOCCP (2007 – 2010). Equivalent simulated values from the IPSL and*
 599 *CNRM models have been added when available.*

600

601

602 **List of figures**

603 **Figure 1:** Area under study. a) Isolines of NCEP precipitable water for entire
604 atmosphere (1984 – 200WSu-cold6), every 3 kg/m², only larger than 35 kg/m² highlighting
605 ITCZ area. Red is July, blue is January. Dotted square is the area of current study, dashed one
606 is the area of KH93 study; b-c) Mean CF_{GOCCP} (2007 – 2010) (DJF-JJA); d) $CF_{GOCCP3D}$ mean
607 vertical profile (2007 – 2010); e-f) same as b-c) for CF_{ISCCP} (1984 – 2006); g-h) for τ , i-j), for
608 *ref*.

609 **Figure 2:** Evolution of the mean cloud properties anomaly from 1984 to 2006. a)
610 CF_{ISCCP} ; b) τ , c) *ref*, d) CF_{ISCCP} from models; e) CF_{GOCCP} from models; e) *ref* from models.
611 Blue for DJF observed, red for JJA observed, black for JJA IPSL model, brown for JJA
612 CNRM model, magenta for DJF IPSL model, green for DJF CNRM model. Horizontal dashed
613 lines correspond to the values of standard deviations. Numbers in the titles are values of
614 trends in 23 years, and the significant ones (i.e. superior to the variability – standard
615 deviation) are in rectangles. Blue vertical lines indicate particular years in DJF, red ones the
616 same in JJA, and black ones particular years in both DJF and JJA.

617 **Figure 3:** Log of percentage of occurrence of SST values (by classes of 1 K) versus
618 w_{500} values (by classes of 10 hPa/day) from 1984 to 2010. a) NCEP in DJF; (b) NCEP in JJA;
619 (c) ERA-Interim in DJF; d) ERA-Interim in JJA; e) IPSL model in DJF; f) IPSL model in
620 JJA; g) CNRM model in DJF; h) CNRM model in JJA. (white horizontal and vertical lines
621 indicate the limits of the five dynamical regimes and the number in white are the percentage
622 of pixels of each regime).

623 **Figure 4:** a-e. Anomaly of the percentage of pixels of each dynamical regime from
624 1984 to 2010 (DJF in blue, JJA in red) defined by NCEP w_{500} and SST values. a) As, b) WSu-
625 cold, c) WSu-warm, d) SSu-cold, e) SSu-warm. The horizontal dashed lines correspond to the
626 values of standard deviations. Values of the trends in 27 years are indicated in the titles for

627 both NCEP and ERA-Interim reanalysis, and the significant ones are in rectangles. Vertical
628 lines are the same as in Fig. 2. f-g. Equivalent trends (the value of the linear regression slope
629 of the curve, multiplied by the number of years) values over 27 years for DJF (f.) and JJA (g.)
630 calculated from NCEP, ERA-Interim, IPSL model, CNRM model. Significant trends are
631 indicated by an arrow.

632 **Figure 5:** Mean values of cloud properties for the five dynamical regimes. Three first
633 lines are CF , τ , and ref in DJF, three last lines the same in JJA. Blue bars are based on NCEP
634 reanalyses, green ones on ERA-Interim reanalyses. Same results from models (IPSL and
635 CNRM) have been added (not colour bars).

636 **Figure 6:** mean vertical profile of $CF_{GOCCP3D}$ (2007 – 2010). The complete database
637 are represented by the black dotted lines, it is then separated onto the five regimes. a) in DJF;
638 b) in JJA. X axis is in logarithmic scale.

639 **Figure 7:** Same as Fig. 5 but for trend values (over 23 years) instead of mean values.
640 A “trend” is the value of the linear regression slope of the curve, multiplied by the number of
641 years. CF_{GOCCP} values are not drawn as there are too few years for trend estimation. Black
642 arrows are added when the trend is superior to the variability (i.e. the standard deviation).
643 Same results from models (IPSL and CNRM) have been added (not colour bars).

644 **Figure A.1:** Satellite viewing angle θ_v (a) example of values in January, (b)
645 percentage of values that are more than 2° lower or larger than the median value for the entire
646 time period, (c) mean value of the difference between θ_v and its median when the percentage
647 of (b) is non-zero.

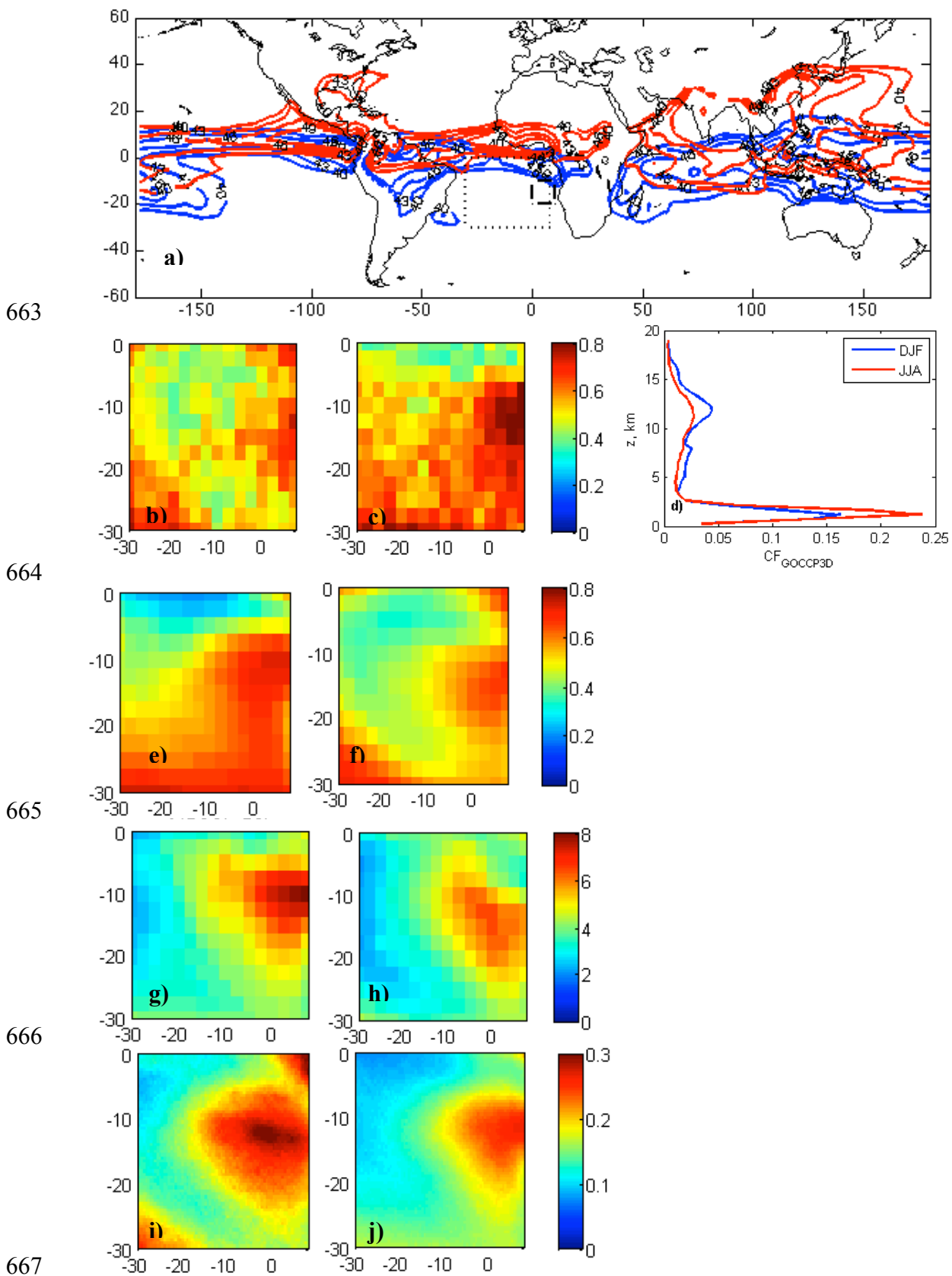
648 **Figure A.2:** Satellite azimuthal relative angle ϕ (a) example of values in January, (b)
649 percentage of values that are more than 5° lower or larger than the median value for the entire
650 time period, (c) mean value of the difference between ϕ and its median when the percentage
651 of (b) is non-zero.

652 **Figure A.3:** (a) Solar zenithal angle at 1200 UTC on January 15th; (b) same as (a) but
653 on July 15th.

654 **Figure A.4:** Simulation of the reflectance as a function of the optical thickness, for
655 four representation of the satellite geometry: solar zenithal angle of 20°/angle of viewing
656 direction with nadir of 15°/relative viewing azimuth angle of 50° (characteristic of January,
657 red plane line), 32°/15°/50° (characteristic of January, blue plane line); 22°/42°/130°
658 (characteristic of July, red dashed line); 50°/42°/130° (characteristic of July, red dashed line).

659 **Figure A.5:** Time evolution of the clear sky reflectance, during the complete period
660 (in blue). Satellite changes are indicated by vertical red lines.

661
662



668 *Figure 1: Area under study. a) Isolines of NCEP precipitable water for entire atmosphere*
 669 *(1984 – 2006), every 3 kg/m², only larger than 35 kg/m² highlighting ITCZ area. Red is July,*
 670 *blue is January. Dotted square is the area of current study, dashed one is the area of KH93*
 671 *study; b-c) Mean CF_{GOCCP} (2007 – 2010) (DJF-JJA); d) CF_{GOCCP3D} mean vertical profile*
 672 *(2007 – 2010); e-f) same as b-c) for CF_{ISCCP} (1984 – 2006); g-h) for τ; i-j), for ref.*

673

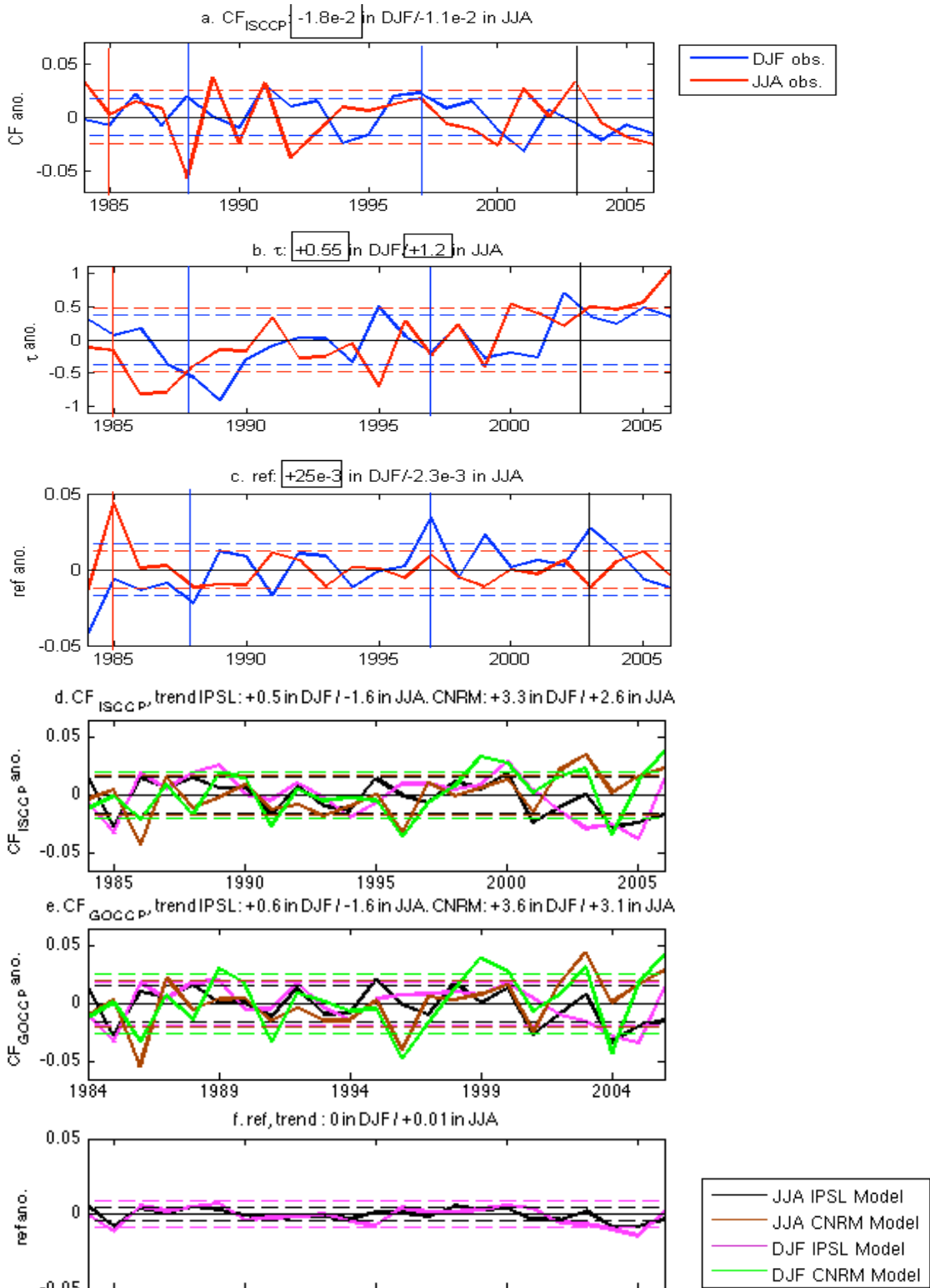
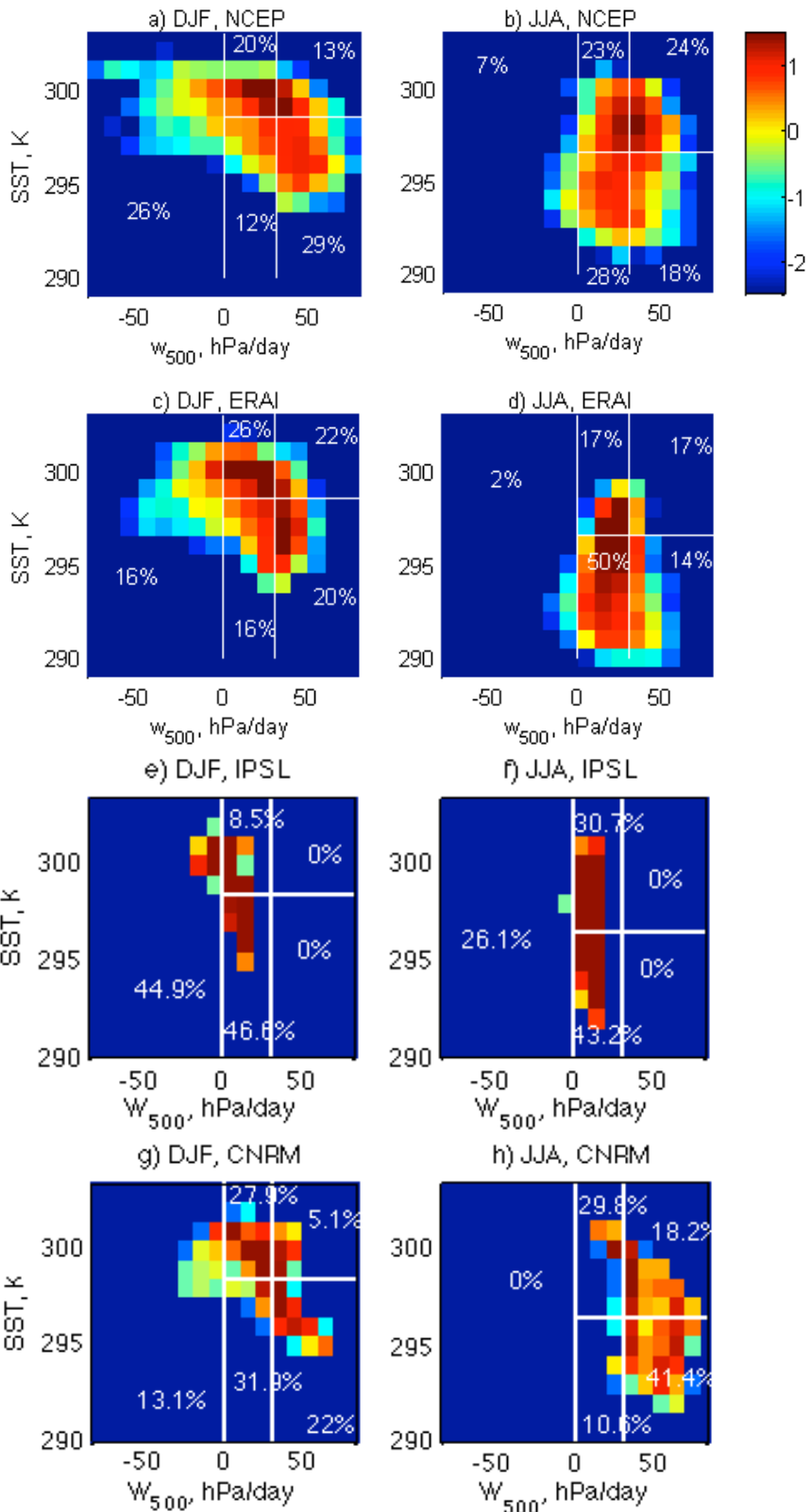


Figure 2: Evolution of the mean cloud properties anomaly from 1984 to 2006. a) CF_{ISCCP} ; b) τ ; c) ref; d) CF_{ISCCP} from models; e) CF_{GOCCP} from models; f) ref from models. Blue for DJF observed, red for JJA observed, black for JJA IPSL model, brown for JJA CNRM model, magenta for DJF IPSL model, green for DJF CNRM model. Horizontal dashed lines correspond to the values of standard deviations. Numbers in the titles are values of trends in 23 years, and the significant ones (i.e. superior to the variability – standard deviation) are in rectangles. Blue vertical lines indicate particular years in DJF, red ones the same in JJA, and black ones particular years in both DJF and JJA.



687

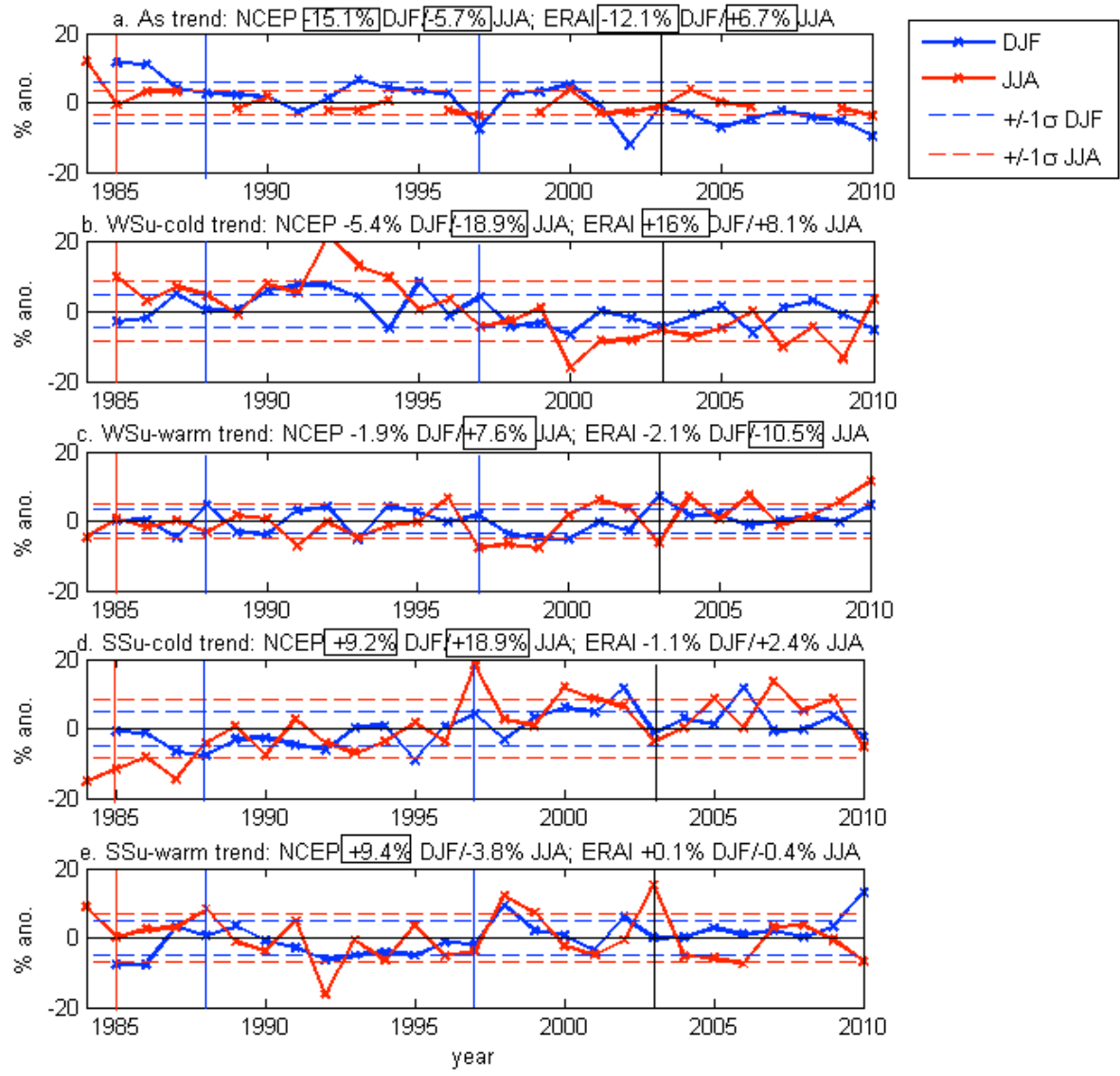
688

689

690

691 *Figure 3: Log of percentage of occurrence of SST values (by classes of 1 K) versus w_{500}*
692 *values (by classes of 10 hPa/day) from 1984 to 2010. a) NCEP in DJF; (b)*
693 *NCEP in JJA; (c) ERA-Interim in DJF; d) ERA-Interim in JJA; e) IPSL model in DJF;*
694 *f) IPSL model in JJA; g) CNRM model in DJF; h) CNRM model in JJA. (white horizontal and vertical lines indicate*
695 *the limits of the five dynamical regimes and the number in white are the percentage of pixels*
696 *of each regime).*

697

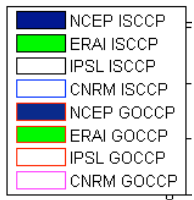


698

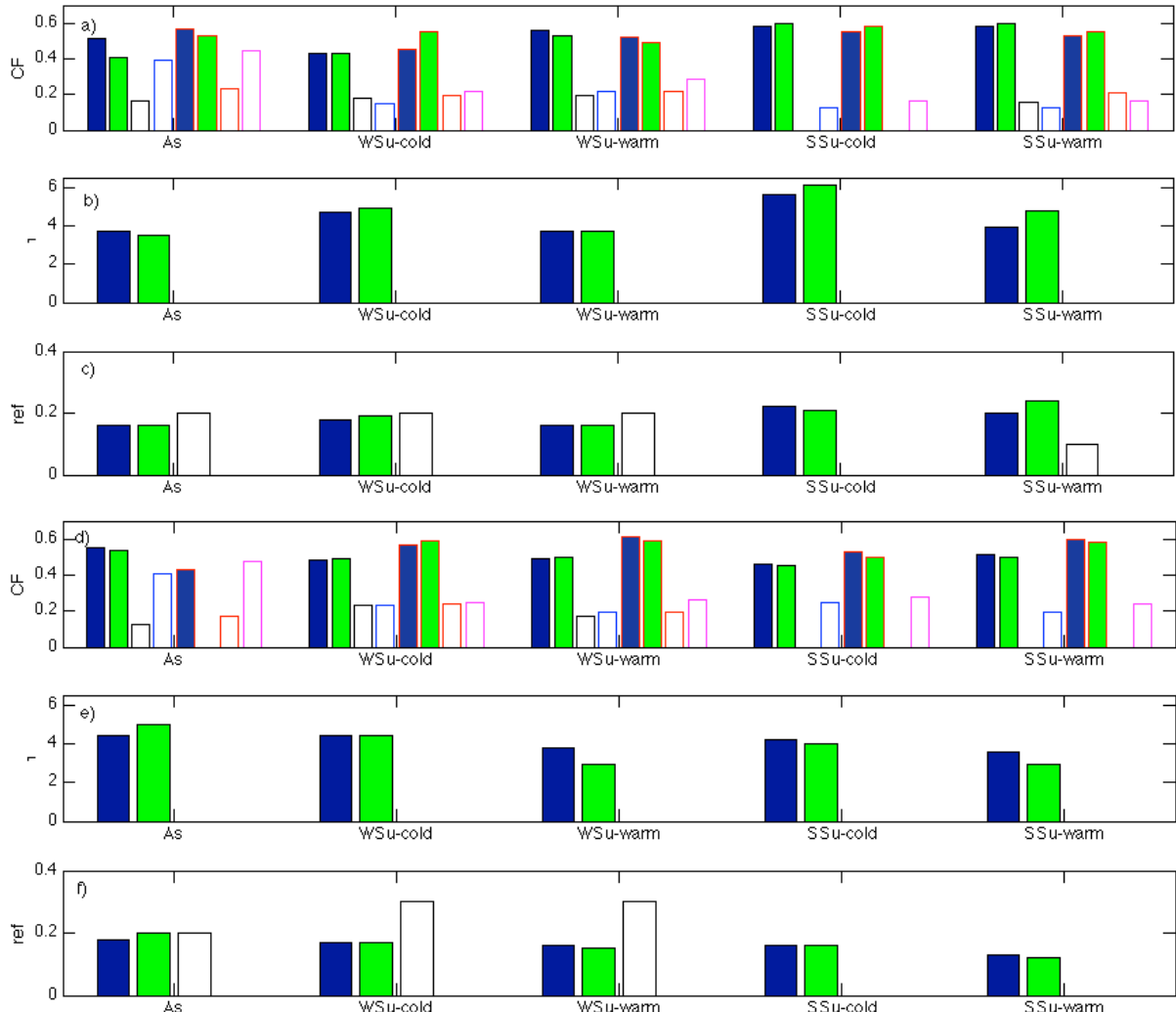
699

700

701 *Figure 4: a-e. Anomaly of the percentage of pixels of each dynamical regime from 1984 to*
 702 *2010 (DJF in blue, JJA in red) defined by NCEP w_{500} and SST values. a) As, b) WSu-cold, c)*
 703 *WSu-warm, d) SSu-cold, e) SSu-warm. The horizontal dashed lines correspond to the values*
 704 *of standard deviations. Values of the trends in 27 years are indicated in the titles for both*
 705 *NCEP and ERA-Interim reanalysis, and the significant ones are in rectangles. Vertical lines*
 706 *are the same as in Fig. 2. f-g. Equivalent trends (the value of the linear regression slope of*
 707 *the curve, multiplied by the number of years) values over 27 years for DJF (f.) and JJA (g.)*
 708 *calculated from NCEP, ERA-Interim, IPSL model, CNRM model. Significant trends are*
 709 *indicated by an arrow.*



710



711

712

713

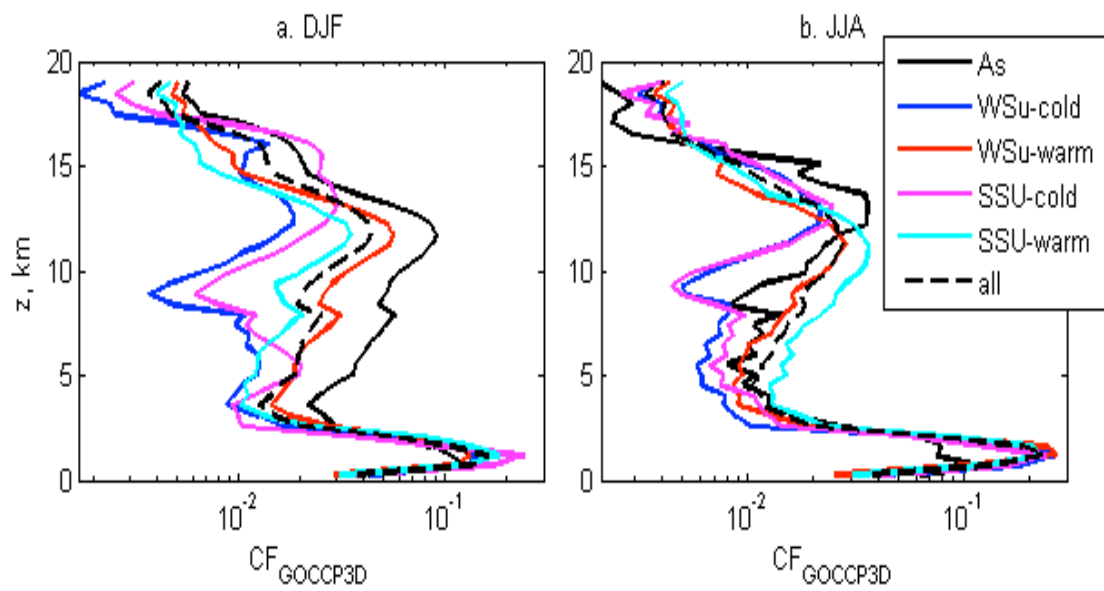
714

715

716

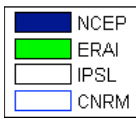
717

Figure 5: Mean values of cloud properties for the five dynamical regimes. Three first lines are CF, τ , and ref in DJF, three last lines the same in JJA. Blue bars are based on NCEP reanalyses, green ones on ERA-Interim reanalyses. Same results from models (IPSL and CNRM) have been added (not colour bars).

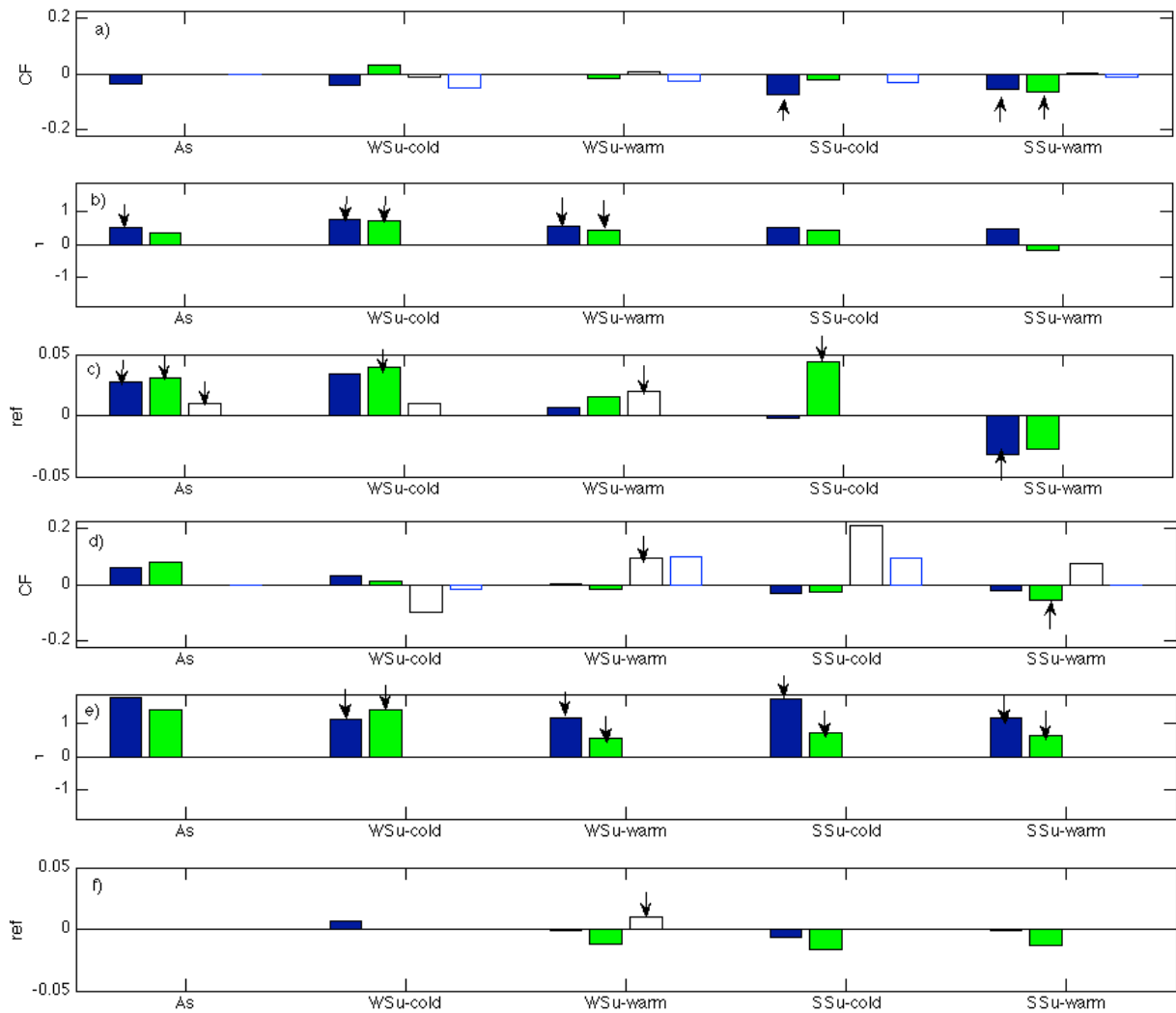


718
 719 *Figure 6: mean vertical profile of $CF_{GOCCP3D}$ (2007 – 2010). The complete database are*
 720 *represented by the black dotted lines, it is then separated onto the five regimes. a) in DJF; b)*
 721 *in JJA. X axis is in logarithmic scale.*

722
 723



724



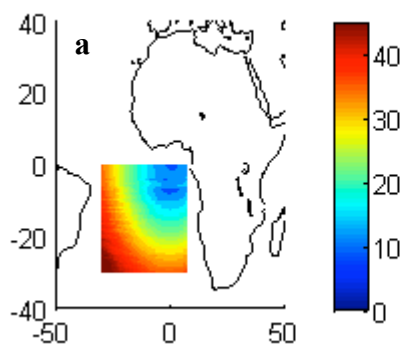
725

726

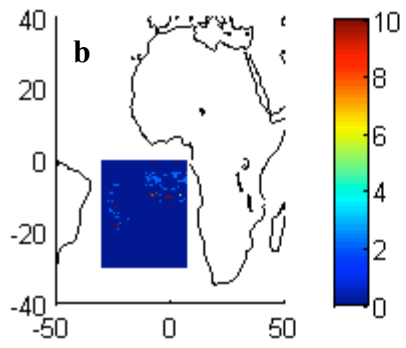
727 *Figure 7: Same as Fig. 5 but for trend values (over 23 years) instead of mean values. A*
728 *“trend” is the value of the linear regression slope of the curve, multiplied by the number of*
729 *years. CF_{GOCCP} values are not drawn as there are too few years for trend estimation. Black*
730 *arrows are added when the trend is superior to the variability (i.e. the standard deviation).*

731 *Same results from models (IPSL and CNRM) have been added (not colour bars).*

732



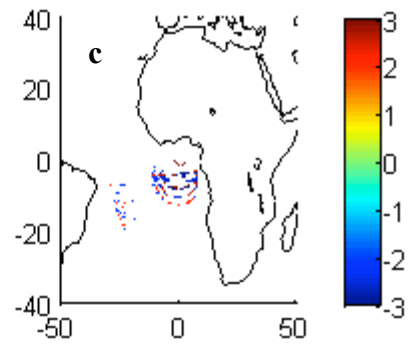
733

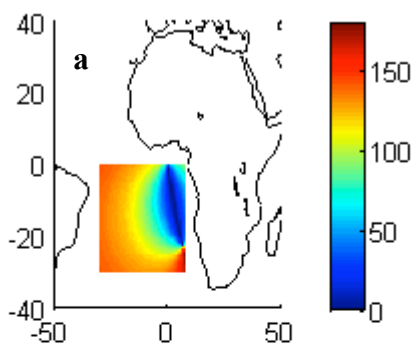


734

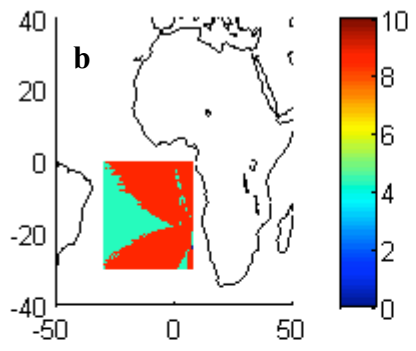
735 *Figure A.1: Satellite viewing angle θ_v (a) example of values in January, (b) percentage of*
 736 *values that are more than 2° lower or larger than the median value for the entire time period,*
 737 *(c) mean value of the difference between θ_v and its median when the percentage of (b) is non-*
 738 *zero.*

739





740



741

742
743
744
745
746

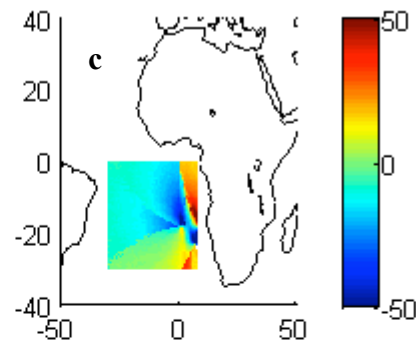
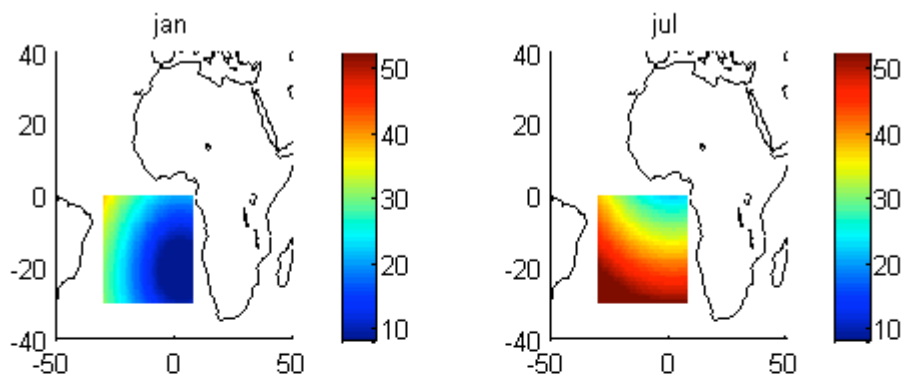
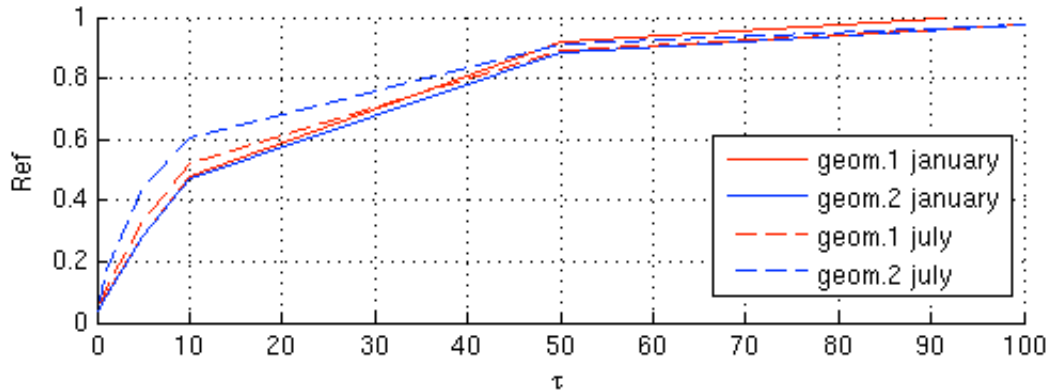


Figure A.2: Satellite azimuthal relative angle ϕ (a) example of values in January, (b) percentage of values that are more than 5° lower or larger than the median value for the entire time period, (c) mean value of the difference between ϕ and its median when the percentage of (b) is non-zero.



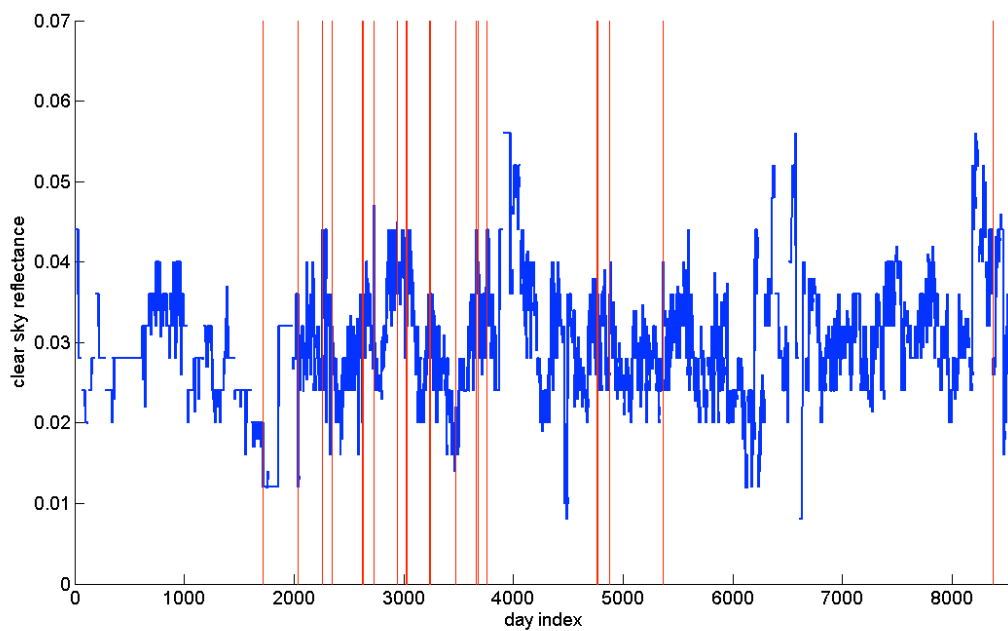
747
748 Figure A.3: (a) Solar zenithal angle at 1200 UTC on January 15th; (b) same as (a) but on July
749 15th.

750



751
752
753
754
755
756

Figure A.4: Simulation of the reflectance as a function of the optical thickness, for four representation of the satellite geometry: solar zenithal angle of 20°/angle of viewing direction with nadir of 15°/relative viewing azimuth angle of 50° (characteristic of January, red plane line); 32°/15°/50° (characteristic of January, blue plane line); 22°/42°/130° (characteristic of July, red dashed line); 50°/42°/130° (characteristic of July, red dashed line).



757
758 *Figure A.5: Time evolution of the clear sky reflectance, during the complete period (in blue).*
759 *Satellite changes are indicated by vertical red lines.*
760
761
762
763
764

765